Verification of electromagnetic fluid-kinetic hybrid electron model in global gyrokinetic particle simulation

I. Holod and Z. Lin
Department of Physics and Astronomy, University of California, Irvine, California 92697, USA

(Received 1 November 2012; accepted 6 March 2013; published online 26 March 2013)

The fluid-kinetic hybrid electron model is verified in global gyrokinetic particle simulation of linear electromagnetic drift-Alfvénic instabilities in tokamak. In particular, we have recovered the β-stabilization of the ion temperature gradient mode, transition to collisionless trapped electron mode, and the onset of kinetic ballooning mode as β_e (ratio of electron kinetic pressure to magnetic pressure) increases. © *2013 American Institute of Physics*. [http://dx.doi.org/10.1063/1.4798392]

I. INTRODUCTION

Plasma confinement and transport depend on nonlinear interactions between multiple physical processes with wide range of spatial and temporal characteristic scales. Thus fully self-consistent simulation of burning plasmas must incorporate global geometry, wave-particle interactions, and cross-scale coupling between micro and meso-scale turbulence. Anomalous transport in tokamak plasmas generated by micro-instabilities can be significantly affected by the presence of magnetic perturbations. The β-stabilization of the ion temperature gradient (ITG) mode,[1,2] and destabilizing of the kinetic ballooning mode (KBM) bellow critical MHD β-limit[3] are just few examples of such influence. Therefore, fully self-consistent simulation must include the finite-β effects in order to properly study the turbulent transport in burning plasmas.

Electromagnetic gyrokinetic simulation incorporating electron dynamics is numerically challenging. The verification of the electromagnetic simulation models is thus important. There are few linear electromagnetic benchmarks between major gyrokinetic codes (in the local limit),[4–6] as well as some nonlinear comparisons.[5] Several global gyrokinetic particle codes also have electromagnetic capabilities,[7–9] but, until now, there are no published electromagnetic cross-verifications among them.

The small electron mass presents a numerical difficulty for simultaneously treating the dynamics of ions and electrons in simulations. A fluid-kinetic hybrid electron model[10] currently implemented in the gyrokinetic toroidal code GTC[11] overcomes this difficulty by expanding the electron drift kinetic equation using the electron-ion mass ratio as a small parameter. The model accurately recovers low frequency plasma dielectric responses and faithfully preserves linear and nonlinear wave-particle resonance. Maximum numerical efficiency is achieved by overcoming the electron Courant condition and suppressing tearing modes and high frequency modes thus effectively suppressing "electron noise." Extension to treat the collisionless tearing modes is currently underway.[12]

The fluid-kinetic hybrid electron model avoids the well-known "cancellation problem" in some gyrokinetic particle and continuum codes.[7,9,13,14] The "cancellation problem" arises when solving a particular form of the Ampère's law, where two large terms are artificially added to the original Ampère's law. These two terms are needed because canonical momentum is used as an independent variable to overcome a numerical difficulty of calculating the inductive electric field by an explicit time derivative. Analytically, these two terms should cancel with each other exactly. However, a small error in numerically evaluating these two large terms can give rise to a residue, which leads to a large error in solving the Ampère's law. In contrast, the fluid-kinetic hybrid electron model is based on the original Ampère's law, which is free from the "cancellation problem."

A single version GTC is currently capable of both full-f and δf simulations, gyrokinetic or fully kinetic ions, kinetic electrons and electromagnetic fluctuations, general toroidal geometry with shaped, up-down asymmetric equilibrium and experimental plasma profiles, equilibrium current for kink drive, multiple ion species, neoclassical effects with Fokker-Planck collision operators conserving particle, momentum and energy, equilibrium radial electric field with toroidal and poloidal rotations, and sources/sinks and external antenna. GTC is a platform-independent program using standard FORTRAN, message passing interface, and OpenMP, and achieves nearly perfect scalability on massively parallel computers, including the world fastest computer with more than 10^5 cores and graphic processing unit acceleration.

GTC has been well benchmarked for electrostatic simulations with kinetic electrons.[15,29] The comparison of linear growth rate and real frequency as a function of η_i between different codes is shown in Fig. 1. Building on the successful and extensive applications to electrostatic micro-turbulence[16] and energetic particle physics,[17] GTC has demonstrated the capability to simulate mesoscale MHD modes such as toroidal Alfvén eigenmode,[18] reversed shear Alfvén eigenmode,[19,20] beta-induced Alfvén eigenmode,[21] and ideal ballooning mode.[22] The kinetic effects of electrons can be important for such low- and intermediate-n electromagnetic modes, e.g., damping effects by trapped electrons.[19] In this work, we present the linear results of electromagnetic gyrokinetic particle simulations of drift-Alfvénic instabilities in order to verify the validity of the fluid-kinetic electron model, especially the kinetic effects for the high-n modes. Verified electrostatic results can serve as a reference point for electromagnetic simulations as $\beta_e = 8\pi n_e T_e / B_0^2$ approaches zero.

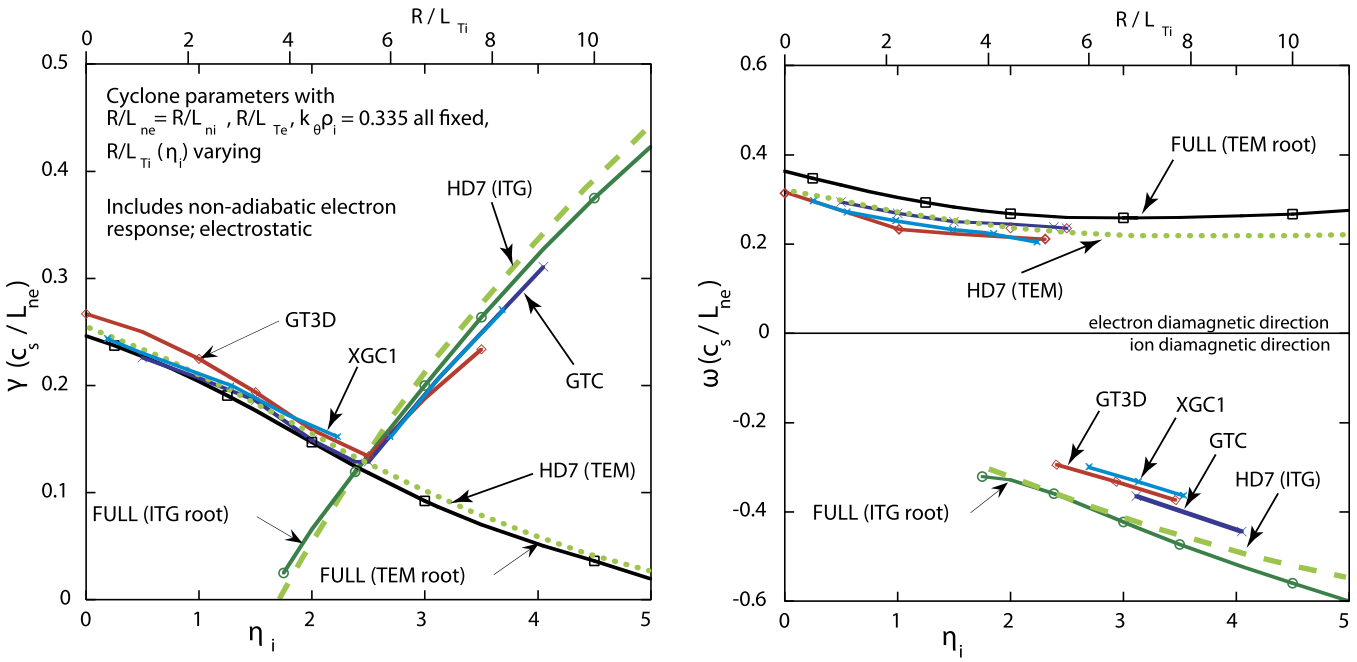

FIG. 1. Linear growth rate γ and real frequency ω of electrostatic ITG and CTEM modes as a function of η_i. GTC, GT3D, and FULL data from Ref. 29, HD7 data from Ref. 31, and XGC1 data from Chang and Ku (Ref. 33).

This paper has the following structure. In Sec. II, we provide a general GTC overview and more detailed formulation of the fluid-kinetic hybrid electron model. Simulation setup and results are discussed in Sec. III, where we present a β_e dependence of mode real frequency and linear growth rate, recovering the β-stabilization of the ITG mode, ITG-CTEM (collisionless trapped electron mode) transition, and the onset of KBM. Section IV concludes with the summary.

II. GTC FORMULATION

The GTC simulates plasma consisting of three particle species: electrons, thermal ions, and energetic particles or impurities. The dynamics of particle's gyrocenter is determined by solving corresponding equations of motion. In addition, the δf method[23] is adopted in which the gyrokinetic equation describing particle's weight is integrated along the perturbed trajectories, to improve numerical efficiency and reduce noise.

The gyrokinetic equation, together with gyrocenter equations of motion describing toroidal plasmas in the inhomogeneous magnetic field, using the gyrocenter position $\mathbf{X}$, magnetic moment μ and parallel velocity $v_\parallel$ as a set of independent variables in the 5D phase space, reads[24]

$$\frac{d}{dt}f_s(\mathbf{X},\mu,v_\parallel,t) \equiv \left[\frac{\partial}{\partial t}+\dot{\mathbf{X}}\cdot\nabla+\dot{v}_\parallel\frac{\partial}{\partial v_\parallel}\right]f_s = 0, \quad (1)$$

$$\begin{aligned}\dot{\mathbf{X}} &= v_\parallel\frac{\mathbf{B}}{B_0}+\mathbf{v}_E+\mathbf{v}_d\\ \dot{v}_\parallel &= -\frac{1}{m_s}\frac{\mathbf{B}^*}{B_0}\cdot(\mu\nabla B_0+Z_s\nabla\phi)-\frac{Z_s}{m_s c}\frac{\partial A_\parallel}{\partial t}.\end{aligned} \quad (2)$$

Here, index $s = i, f, e$ stands for the particle species, Z_s is the particle charge, and m_s is the particle mass, $\mathbf{B}_0 \equiv B_0\mathbf{b}_0$ is the equilibrium magnetic field, $\mathbf{B} \equiv \mathbf{B}_0 + \delta\mathbf{B}$, and

$$\mathbf{B}^* = \mathbf{B}_0^* + \delta\mathbf{B} = \mathbf{B}_0 + \frac{B_0 v_\parallel}{\Omega_s}\nabla\times\mathbf{b}_0 + \delta\mathbf{B}.$$

Other terms in Eq. (2) are the $E\times B$ drift velocity

$$\mathbf{v}_E = \frac{c\mathbf{b}_0\times\nabla\phi}{B_0}$$

and magnetic drift velocity

$$\mathbf{v}_d = \mathbf{v}_c + \mathbf{v}_g,$$

where the magnetic curvature drift is

$$\mathbf{v}_c = \frac{v_\parallel^2}{\Omega_s}\nabla\times\mathbf{b}_0,$$

and the grad-B drift is

$$\mathbf{v}_g = \frac{\mu}{m_s\Omega_s}\mathbf{b}_0\times\nabla B_0.$$

In our description, we exclude the compressional component of the magnetic field perturbation by assuming $\delta B_\parallel = 0$, thus

$$\delta\mathbf{B} = \delta\mathbf{B}_\perp = \nabla\times\lambda\mathbf{B}_0, \quad (3)$$

with $\lambda = A_\parallel/B_0$.

In Eq. (1), the electrostatic potential ϕ and vector potential $A_\parallel$ represent corresponding gyroaveraged values for ions.

A. Fluid-kinetic hybrid electron model

The fluid-kinetic hybrid electron model[10] is developed to improve the numerical properties of simulations with kinetic electrons for the micro- and meso-scale turbulence. The idea of hybrid method is in the expansion of the electron response

into a dominant adiabatic part and a high-order kinetic perturbation, based on the small electron-ion mass ratio.

In the lowest order, adiabatic part is described as a massless fluid using continuity equation. In the higher order, the fluid response is corrected by subtracting from it the non-adiabatic part which is treated kinetically with all the nonlinear effects preserved. Using the fluid-kinetic hybrid electron model avoids dealing with the electron Courant condition and unnecessary high-frequency modes. This model is the most efficient electron model for kinetic simulations of electromagnetic turbulence in the absence of tearing modes.

The electron perturbed distribution function can be expanded using a small parameter $\delta_m \equiv \sqrt{m_e/\beta_e m_i} \sim \omega/k_\parallel v_\parallel$, such that

$$f_e = f_{0e} + \delta f_e^{(0)} + \delta h_e. \tag{4}$$

Here, f_{0e} is the equilibrium distribution satisfying

$$(v_\parallel \hat{\mathbf{b}}_0 + \mathbf{v}_d) \cdot \nabla f_{0e} - \frac{\mu}{m_e}\frac{\mathbf{B}_0^*}{B_0} \cdot \nabla B_0 \frac{\partial f_{0e}}{\partial v_\parallel} = 0. \tag{5}$$

The solution for $\delta f_e^{(0)}$ can be found from the electron drift-kinetic equation (1), keeping just the lowest order terms

$$v_\parallel \mathbf{b}_0 \cdot \nabla \delta f_e^{(0)} = -v_\parallel \frac{\delta \mathbf{B}_\perp}{B_0} \cdot \nabla f_{0e}|_{v_\perp} + v_\parallel f_{0e} \frac{e}{T_{0e}} \mathbf{b}_0 \cdot \nabla \delta \phi_{\text{eff}}, \tag{6}$$

where the equilibrium distribution f_{0e} is assumed to be Maxwellian for the parallel velocity, with no inhomogeneity along the magnetic field lines, and the effective potential $\delta\phi_{\text{eff}}$ is determining the parallel electric field

$$\delta E_\parallel = -\hat{\mathbf{b}} \cdot \nabla \delta \phi_{\text{eff}}.$$

The continuous solution of Eq. (6) is

$$\frac{\delta f_e^{(0)}}{f_{0e}} = \frac{e\delta\phi_{\text{eff}}}{T_{0e}} + \frac{\partial \ln f_{0e}}{\partial \psi}\bigg|_{v_\perp} \delta\psi + \frac{\partial \ln f_{0e}}{\partial \alpha}\bigg|_{v_\perp} \delta\alpha, \tag{7}$$

describing the adiabatic electron response, i.e., electrons are isothermal along the perturbed magnetic field line, with the Boltzmann response to scalar potential. In deriving Eq. (7), we have used the Clebsch representation for the toroidal magnetic field

$$\mathbf{B} = \mathbf{B}_0 + \delta\mathbf{B}_\perp = \nabla(\psi + \delta\psi) \times \nabla(\alpha + \delta\alpha), \tag{8}$$

where ψ and $\alpha = q(\psi)\theta - \zeta$ are equilibrium poloidal flux and magnetic field line label respectively, with θ and ζ being the poloidal and toroidal angles in magnetic coordinates.

Since the electron response (7) is adiabatic only for non-zonal ($k_\parallel \neq 0$) modes, Eq. (6) excludes zonal components (with $k_\parallel = 0$) of the perturbed potentials. Zonal fields are solved separately.[8,25]

In the hybrid scheme, the adiabatic density response obtained by integrating Eq. (7) over the velocity space is used to calculate the effective potential

$$\frac{e\delta\phi_{\text{eff}}}{T_{0e}} = \frac{\delta n_e^{(0)}}{n_{0e}} - \frac{\partial \ln n_{0e}}{\partial \psi}\delta\psi + \frac{\partial \ln n_{0e}}{\partial \alpha}\delta\alpha, \tag{9}$$

where

$$\delta n_e^{(0)} = \delta n_e - \int d\mathbf{v} \delta h_e. \tag{10}$$

The non-adiabatic part of the electron distribution function δh_e is obtained from the drift-kinetic equation (1), taking into account Eqs. (4)–(6)

$$\frac{1}{f_{0e}}\frac{d\delta h_e}{dt} = -\mathbf{v}_E \cdot \nabla \ln f_{0e}|_{v_\perp} - \frac{\partial}{\partial t}\frac{\delta f_e^{(0)}}{f_{0e}} - \mathbf{v}_d \cdot \nabla \frac{\delta f_e^{(0)}}{f_{0e}} + \frac{e}{T_{0e}}\mathbf{v}_d \cdot \nabla\phi - \frac{c\mathbf{b}_0 \times \nabla\langle\phi\rangle}{B_0} \cdot \nabla \frac{\delta f_e^{(0)}}{f_{0e}} + \frac{ev_\parallel}{cT_{0e}}\frac{\partial\langle A_\parallel\rangle}{\partial t}, \tag{11}$$

where the angular brackets denote zonal components of the perturbed potentials.

Equations (9)–(11) are solved iteratively. At the first iteration, we use $\delta n_e^{(0)} = \delta n_e$ to find $\delta\phi_{\text{eff}}$, which is then used in the right hand side of Eq. (11) to calculate the kinetic correction δh_e.

The perturbed density δn_e is calculated using the electron continuity equation, obtained by integrating the drift-kinetic equation (1) over the velocity space

$$\frac{\partial \delta n_e}{\partial t} + \mathbf{B}_0 \cdot \nabla\left(\frac{n_e \delta u_{||e}}{B_0}\right) + \delta\mathbf{B}_\perp \cdot \nabla\left(\frac{n_{0e}\delta u_{||e}}{B_0}\right) + B_0 \mathbf{v}_E \cdot \nabla n_e - (n_{0e}\mathbf{v}_* + 2n_e\mathbf{v}_E) \cdot \frac{\nabla B_0}{B_0} = 0, \tag{12}$$

where

$$\mathbf{v}_* = -\frac{1}{n_{0e}B_0}\mathbf{b}_0 \times \nabla(\delta P_{||e} + \delta P_{\perp e}),$$

and the perturbed pressure

$$\delta P_{\perp e} = \int d\mathbf{v}\mu B_0 \delta f_e = n_{0e}\delta\phi_{\text{eff}} + \frac{\partial P_{0e}}{\partial\psi}\delta\psi + \int d\mathbf{v}\mu B_0 \delta h_e,$$
$$\delta P_{||e} = \int d\mathbf{v} m_e v_\parallel^2 \delta f_e = n_{0e}\delta\phi_{\text{eff}} + \frac{\partial P_{0e}}{\partial\psi}\delta\psi + \int d\mathbf{v} m_e v_\parallel^2 \delta h_e,$$

with

$$P_{0e} = n_{0e}T_{0e}.$$

More general formulation of Eq. (12) including the effect of equilibrium current can be found in Ref. 25.

The electron current is determined from the Ampère's law

$$en_e\delta u_{||e} = \frac{c}{4\pi}\nabla_\perp^2 \delta A_\parallel + \sum_{s\neq e} Z_s n_s \delta u_{||s}, \tag{13}$$

while the parallel component of vector potential is found using the Faraday's law

$$\frac{1}{c}\frac{\partial \delta A_\parallel}{\partial t} = -\delta E_\parallel - \mathbf{b}_0 \cdot \nabla \delta\phi = \mathbf{b}_0 \cdot \nabla(\delta\phi_{\text{eff}} - \delta\phi) \equiv \mathbf{b}_0 \cdot \nabla \phi_{\text{ind}}. \tag{14}$$

Note that using Faraday's law to calculate the parallel vector potential, although being very computationally efficient, excludes even (tearing) parity of $\delta A_\parallel$. Alternatively, one may calculate the electron current from the nonadiabatic response δh_e and use the Ampère's law to find $\delta A_\parallel$, as it is done in the split-weight approach.[26]

The nonzonal electrostatic potential $\delta\phi$ is found by solving the gyrokinetic Poisson's equation[27] formulated for multiple ion species

$$\sum_{s\neq e}(\delta\phi - \delta\tilde{\phi}_s)\frac{n_{0s}Z_s^2}{T_{0s}} = \sum_{s\neq e}\bar{n}_s Z_s - en_e, \tag{15}$$

where

$$\delta\bar{n}_s = \int d\mathbf{Z}\delta^3(\mathbf{X}+\rho-\mathbf{x})\delta f_s(\mathbf{Z}),$$

and

$$\delta\tilde{\phi}_s = \int d\mathbf{Z}\delta^3(\mathbf{X}+\rho-\mathbf{x})\delta\bar{\phi}(\mathbf{X})\frac{f_{0s}(\mathbf{Z})}{n_{0s}}.$$

The magnetic field line perturbations $\delta\psi$ and $\delta\alpha$ are related to the parallel vector potential, and, taking into account Eq. (14), can be found from

$$\begin{aligned}\frac{\partial\delta\psi}{\partial t} &= -c\frac{\partial\phi_{\text{ind}}}{\partial\alpha},\\ \frac{\partial\delta\alpha}{\partial t} &= c\frac{\partial\phi_{\text{ind}}}{\partial\psi}.\end{aligned} \tag{16}$$

III. SIMULATION RESULTS

To verify the electron model used in the GTC, we run series of linear simulations using the Cyclone Base Case parameters[28] for the background plasmas. These are $R_0/L_{Ti} = R_0/L_{Te} = 6.9, R_0/L_{ni} = R_0/L_{ne} = 2.2$, and $T_e = T_i$. The inverse aspect ratio is $a/R_0 = 0.36$, where R_0 and a are the tokamak major and minor radii, respectively. Diagnostic is taken at the radial position $r/a = 0.5$, where $q = 1.4$ and $\hat{s} = 0.78$. In the simulations, all ions are protons. For trapped electrons, the higher-order kinetic correction is taken into account using realistic mass ratio $m_e = 5.45\times10^{-4}m_p$. We only consider perturbations with fixed toroidal mode number $n = 10$ which corresponds to the fastest growing mode of $k_\theta\rho_i = 0.22$. The simplified $s-\alpha$ equilibrium model with circular cross-section is used in current simulations.

We start with the convergence study to determine the necessary device size for recovering the local flux-tube results. The dependency of the real frequency and linear growth rate of electrostatic ITG mode on the radial system size (Fig. 2) shows saturation at near $a/\rho_i = 125$ which is used for further simulations. The convergent time step used in the simulations is $\Delta t = 0.005R_0/c_s$. We use the equal grid size in the radial and poloidal directions $\Delta r \approx r\Delta\theta \approx \rho_i$ and 32 grid points in the toroidal directions. The number of particles per cell is 20 for both electrons and ions.

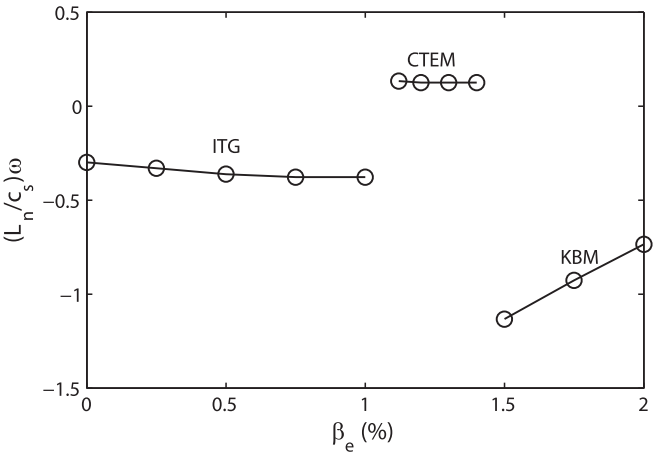

FIG. 3. Real frequency ω of $k_\theta\rho_s = 0.22$ electromagnetic mode as a function of β_e.

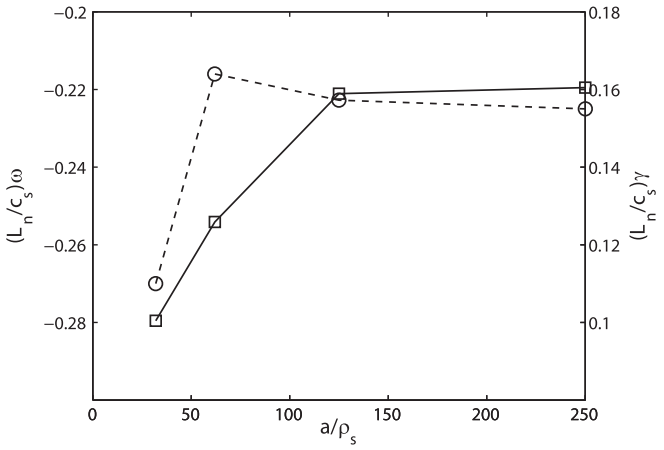

FIG. 2. Real frequency ω (dashed line) and linear growth rate γ (solid line) of $k_\theta\rho_s = 0.22$ electrostatic ITG mode as a function of simulated device size.

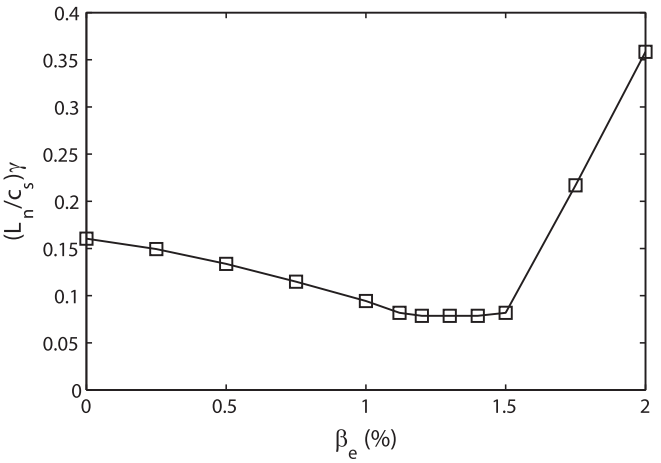

FIG. 4. Linear growth rate γ of $k_\theta\rho_s = 0.22$ electromagnetic mode as a function of β_e.

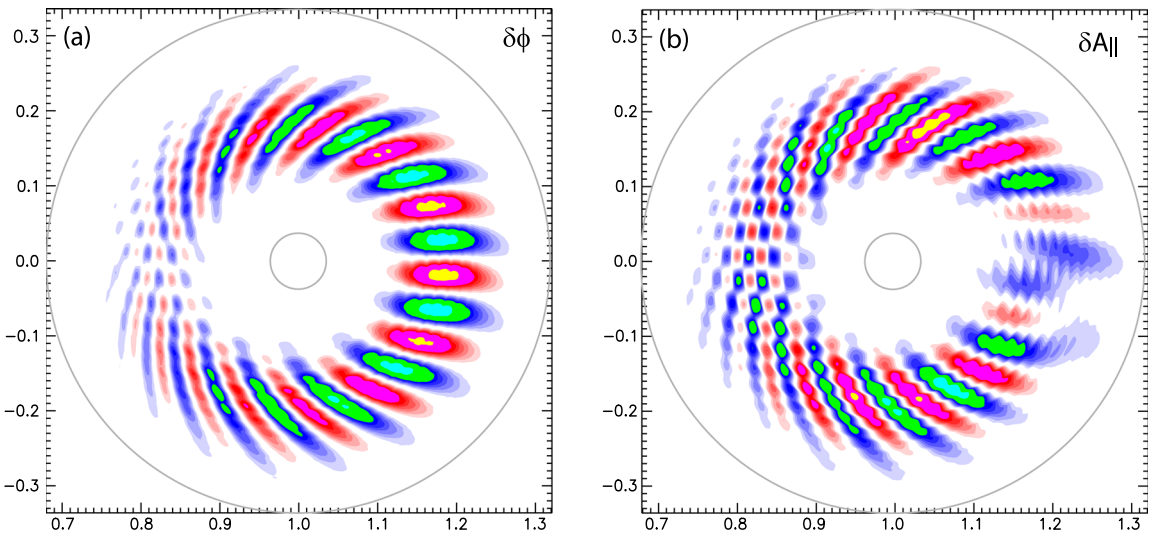

FIG. 5. Poloidal snapshot of electrostatic potential $\delta\phi$ (a) and parallel vector potential $\delta A_{||}$ (b) for electromagnetic ITG mode taken at $\beta_e = 0.5\%$.

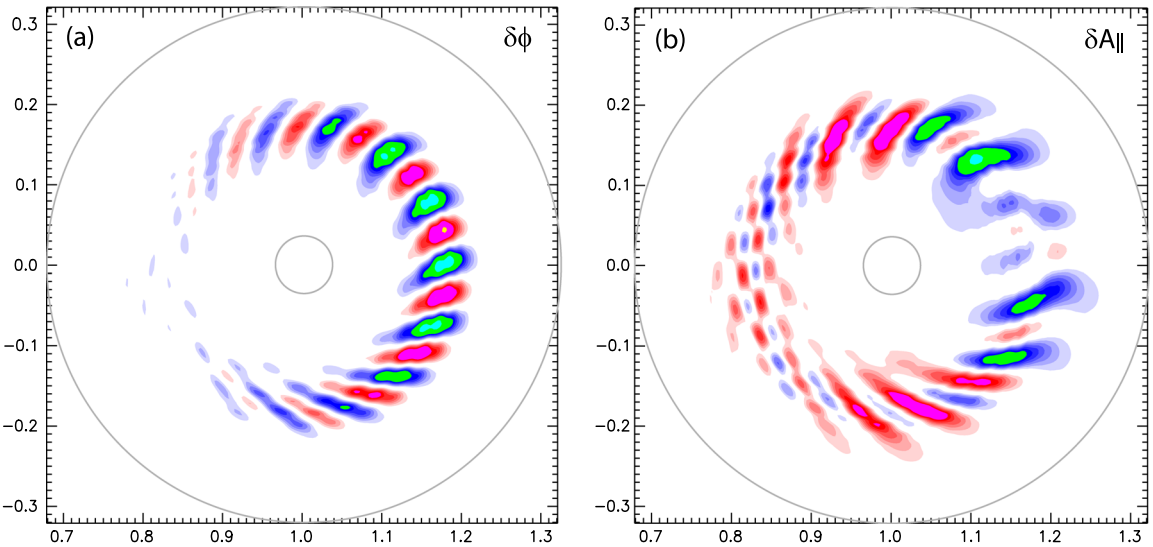

FIG. 6. Poloidal snapshot of electrostatic potential $\delta\phi$ (a) and parallel vector potential $\delta A_{||}$ (b) for electromagnetic CTEM mode taken at $\beta_e = 1.3\%$.

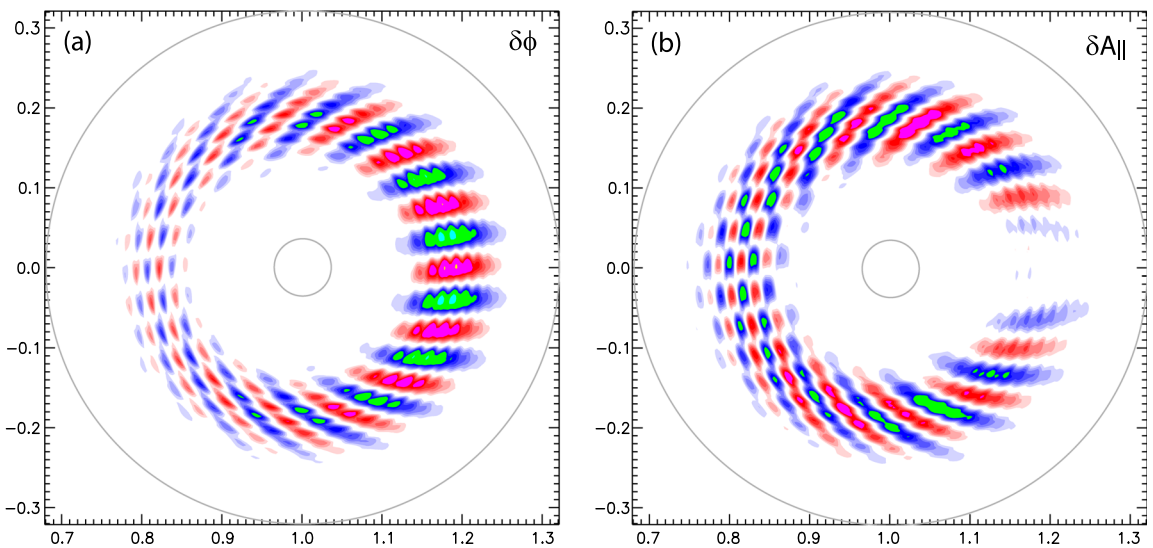

FIG. 7. Poloidal snapshot of electrostatic potential $\delta\phi$ (a) and parallel vector potential $\delta A_{||}$ (b) for KBM mode taken at $\beta_e = 1.75\%$.

The verification of the electromagnetic fluid-kinetic hybrid electron model is performed by running simulations with different on-axis electron density, which corresponds to varying β_e. The electrostatic regime represents the limiting case of $\beta_e = 0$. The dependence of the linear growth rate and real frequency is show in Figs. 4 and 3, respectively. In Fig. 4, we can observe the initial reduction of the growth rate as β_e increases, which corresponds to the effect of β-stabilization of the ITG mode[1,2] (negative real frequency in Fig. 3, corresponding to the ion diamagnetic direction). As β_e approaches zero, both real frequency and linear growth rate approach electrostatic limit recovering previously published results.[15,29] The mode has a distinct ballooning structure as shown in Fig. 5. At $\beta_e \sim 1.15\%$ the ITG growth rate becomes equal to the growth rate of the CTEM[30] which later becomes dominant (switch to the positive real frequency in Fig. 3). The poloidal mode structure at $\beta_e = 1.3\%$ is shown in Fig. 6. At $\beta_e \sim 1.5\%$, the growth rate of the KBM increases sufficiently to become dominant and another switch in the real frequency sign occurs. The growth rate of the KBM mode continues to increase as β_e further increases. The poloidal mode structure at $\beta_e = 1.75\%$ is shown in Fig. 7.

IV. SUMMARY

In this work, we have demonstrated the results of electromagnetic simulation of the linear drift-Alfvénic microinstability. The dependency of the growth rate and real frequency on β_e demonstrates the stabilization of ITG mode, transition to the CTEM, and the onset of KBM mode. This is in agreement with previously published results of gyrokinetic flux-tube simulations with full drift-kinetic electron description.[5,32] As β_e approaches zero, the growth rate and real frequency reach their electrostatic values. Obtained results verify the validity of the fluid-kinetic hybrid electron model for linear global simulation of drift-Alfvénic instabilities in tokamak.

ACKNOWLEDGMENTS

The authors thank J. Q. Dong, C. S. Chang, and S. H. Ku for providing data in Fig. 1. This work was supported by U.S. DOE Center for Gyrokinetic Simulations of Energetic Particles and DOE Grant No. DE-FG02-07ER54916.

[1]B. G. Hong, W. Horton, and D.-I. Choi, Plasma Phys. Controlled Fusion **31**, 1291 (1989).
[2]J. Weiland and A. Hirose, Nucl. Fusion **32**, 151 (1992).
[3]M. S. Chu, C. Chu, G. Guest, J. Y. Hsu, and T. Ohkawa, Phys. Rev. Lett. **41**, 247 (1978).
[4]C. Bourdelle, W. Dorland, X. Garbet *et al.*, Phys. Plasmas **10**, 2881 (2003).
[5]M. J. Pueschel, M. Kammerer, and F. Jenko, Phys. Plasmas **15**, 102310 (2008).
[6]E. Wang, X. Xu, J. Candy *et al.*, Nucl. Fusion **52**, 103015 (2012).
[7]Y. Chen and S. E. Parker, J. Comput. Phys. **189**, 463–475 (2003).
[8]I. Holod, W. L. Zhang, Y. Xiao, and Z. Lin, Phys. Plasmas **16**, 122307 (2009).
[9]A. Bottino, B. Scott, S. Brunner *et al.*, IEEE Trans. Plasma Sci. **38**, 2129 (2010).
[10]Z. Lin and L. Chen, Phys. Plasmas **8**, 1447 (2001).
[11]Z. Lin, T. S. Hahm, W. W. Lee, W. M. Tang, and R. B. White, Science **281**, 1835 (1998).
[12]D. J. Liu and L. Chen, Plasma Phys. Controlled Fusion **53**, 062002 (2011).
[13]J. Candy and R. E. Waltz, J. Comput. Phys. **186**, 545 (2003).
[14]R. Hatzky, A. Konies, and A. Mishchenko, J. Comput. Phys. **225**, 568–590 (2007).
[15]Z. Lin, Y. Nishimura, Y. Xiao, I. Holod, W. L. Zhang, and L. Chen, Plasma Phys. Controlled Fusion **49**, B163 (2007).
[16]I. Holod, Z. Lin, and Y. Xiao, Phys. Plasmas **19**, 012314 (2012).
[17]W. Zhang, Z. Lin, and L. Chen, Phys. Rev. Lett. **101**, 095001 (2008).
[18]W. L. Zhang, I. Holod, Z. Lin, and Y. Xiao, Phys. Plasmas **19**, 022507 (2012).
[19]W. Deng, Z. Lin, I. Holod, Z. Wang, Y. Xiao, and H. Zhang, Nucl. Fusion **52**, 043006 (2012).
[20]D. A. Spong *et al.*, Phys. Plasmas **19**, 082511 (2012).
[21]H. S. Zhang, Z. Lin, and I. Holod, Phys. Rev. Lett. **109**, 025001 (2012).
[22]Z. Li, G. Sun, I. Holod, Y. Xiao, W. Zhang, and Z. Lin, "GTC simulation of ideal ballooning mode in tokamak plasmas," Plasma Sci. Technol. (in press).
[23]G. Hu and J. A. Krommes, Phys. Plasmas **1**, 863 (1994).
[24]A. J. Brizard and T. S. Hahm, Rev. Mod. Phys. **79**, 421 (2007).
[25]W. Deng, Z. Lin, and I. Holod, Nucl. Fusion **52**, 023005 (2012).
[26]W. W. Lee, J. L. V. Lewandowski, T. S. Hahm, and Z. Lin, Phys. Plasmas **8**, 4435 (2001).
[27]W. W. Lee, J. Comput. Phys. **72**, 243 (1987).
[28]A. M. Dimits, G. Bateman, M. A. Beer *et al.*, Phys. Plasmas **7**, 969 (2000).
[29]G. Rewoldt, Z. Lin, and Y. Idomura, Comput. Phys. Commun. **177**, 775 (2007).
[30]Y. Xiao and Z. Lin, Phys. Rev. Lett. **103**, 085004 (2009).
[31]J. Q. Dong, S. M. Mahajan, and W. Horton, Phys. Plasmas **4**, 755 (1997).
[32]J. Candy, Phys. Plasmas **12**, 072307 (2005).
[33]C. S. Chang and S. H. Ku (private communication).